Two-layer formulation for long-runout turbidity currents: theory and bypass flow case

Hongbo Ma[1]†, Gary Parker[2], Matthieu Cartigny[3], Enrica Viparelli[4], S. Balachandar[5], Xudong Fu[1] and Rossella Luchi[6]

[1]Department of Hydraulic Engineering, Key Laboratory of Hydrosphere Sciences of the Ministry of Water Resources, State Key Laboratory of Hydroscience and Enigineering, Tsinghua University, Beijing 100084, China

[2]Department of Earth Science and Environmental Change and Department of Civil and Environmental Engineering, University of Illinois Urbana-Champaign, Urbana, IL 61801, USA

[3]Department of Geography, Durham University, Durham DH1 3LE, UK

[4]Department of Civil Engineering, University of South Carolina, Columbia, SC 29208, USA.

[5]Department of Mechanical and Aerospace Engineering, University of Florida, Gainesville, FL 32611, USA

[6]Hydrodata, Torino 10123, Italia

† Email address for correspondence: bigmatton@gmail.com

Two-layer formulation for long-runout turbidity currents: theory and bypass flow case

Hongbo Ma[1] †, Gary Parker[2], Matthieu Cartigny[3], Enrica Viparelli[4], S. Balachandar[5], Xudong Fu[1] and Rossella Luchi[6]

[1]Department of Hydraulic Engineering, Key Laboratory of Hydrosphere Sciences of the Ministry of Water Resources, State Key Laboratory of Hydroscience and Enigineering, Tsinghua University, Beijing 100084, China

[2]Department of Earth Science and Environmental Change and Department of Civil and Environmental Engineering, University of Illinois Urbana-Champaign, Urbana, IL 61801, USA

[3]Department of Geography, Durham University, Durham DH1 3LE, UK

[4]Department of Civil Engineering, University of South Carolina, Columbia, SC 29208, USA.

[5]Department of Mechanical and Aerospace Engineering, University of Florida, Gainesville, FL 32611, USA

[6]Hydrodata, Torino 10123, Italia

(Received xx; revised xx; accepted xx)

Turbidity currents, which are stratified, sediment-laden bottom flows in the ocean or lakes, can run out for 100's to 1000's of kilometers in submarine channels without losing their stratified structure. Here we derive a layer-averaged, two-layer model for turbidity currents, specifically designed to capture long-runout. Previous models have captured runout only 10's of kilometers, beyond which thickening of the flows becomes excessive and the models without a lateral overspill mechanism fail. In our framework, a lower layer containing nearly all the sediment is a faster, gravity-driven flow that propels an upper layer, where sediment concentration is nearly zero. The thickness of the lower layer is controlled by a competition between interfacial water entrainment due to turbulent mixing and water detrainment due to sediment settling at the interface. The detrainment mechanism, first identified in experiments, is the key feature that prevents excessive thickening of the lower layer and allows long-runout. Under normal flow conditions, we obtain an exact solution to the two-layer formulation revealing a constant velocity and a constant thickening rate in each of the two layers. Numerical simulations applied to gradually varied flows on both constant and exponentially declining bed slopes, with boundary conditions mimicking field observations, show that the predicted lower layer thickness after 200-km flow propagation compares with observed submarine channel depths, whereas previous models overestimate this thickness by 3-4 fold. This formulation opens new avenues for modeling the fluid mechanics and morphodynamics of long-runout turbidity currents in the submarine setting.

† Email address for correspondence: bigmatton@gmail.com

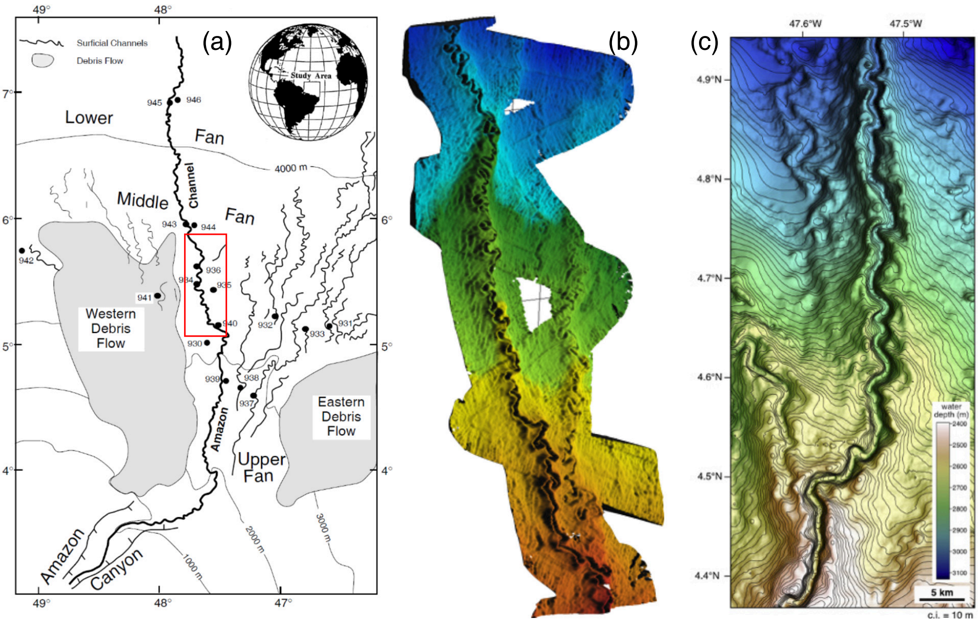

Figure 1: Amazon Submarine Fan and Channels. (*a*) The fan itself (after Mikkelsen *et al.* 1997); (*b*) A ~200 km long reach of the submarine channel (the red box in 1a) (from IFREMER, France);(*c*) Detailed view of the meandering channel (NOAA after Deptuck & Sylvester 2017)

1. Introduction: submarine fans and long-runout turbidity currents

Submarine, or deep-sea fans represent the major ultimate sinks for terrestrial sediment. Sediment is transported across these fans through submarine channels that may extend for hundreds to thousands of kilometers into water that is up to thousands of meters deep. The longest of these fans is the Bengal Fan ~ 3000 km (Curray *et al.* 2002; Schwenk *et al.* 2003). Other very large fans include Congo Fan ~ 1000 km (Picot *et al.* 2016); Indus Fan ~ 1500 km; Amazon Fan ~ 700 km; Mississippi Fan ~ 500 km; Rhone Fan ~ 400 km (Wetzel 1993; Deptuck & Sylvester 2017). Submarine fan systems are emplaced largely by sediment transported through submarine channels, which both convey and are constructed by turbidity currents, i.e. dense bottom flows that obtain their driving power from suspended sediment (Daly 1936; Kuenen 1938; Pirmez & Imran 2003). The channels are commonly highly sinuous (Imran *et al.* 1999; Schwenk *et al.* 2003) and build the fan itself by avulsing across the fan surface (Jobe *et al.* 2020).

Views of the Amazon Submarine Fan and the meandering Amazon Channel itself are given in figure 1. The sinuosity of this channel, and many other channels on submarine fans, implies that their down-channel lengths may notably exceed the length of the fan itself.

Covault *et al.* (2011) have documented 20 long profiles of submarine channels as they traverse an upstream canyon and emanate onto the fan below (figure 2a). Eight of these are 200 km or more in length. It can be seen from the figure that channels on canyon-fan systems have long profiles that vary from approximately constant slopes to strongly upward concave.

Figure 2b shows the along-channel profile of the Amazon Channel of figure 1, including channel thalweg, levee crest and canyon top. Distances are measured down-channel and thus include the effect of sinuosity. The reach in the submarine canyon is 120 km long, and downstream reach on the submarine fan is 760 km long. Bed slope ranges from about 0.014 upstream to about 0.002 downstream.

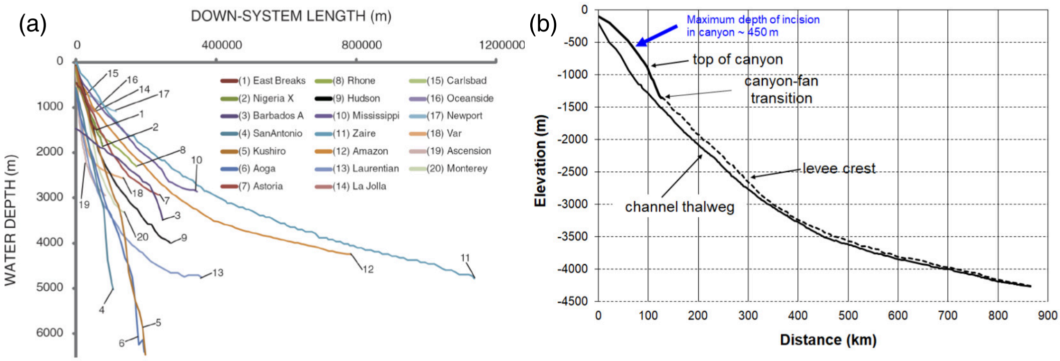

Figure 2: (*a*) Down-channel long profiles of 20 canyon-fan systems (after Covault *et al.* 2011); (*b*) Long profiles of channel thalweg, levee crest and top of canyon for the Amazon Channel of Figure 1. The channel is confined within the Amazon Canyon for the first 120 km, and then extends out 760 km on the fan. The distances are measured along the channel thalweg (based on Pirmez & Imran 2003).

The turbidity currents that excavate submarine canyons and emplace submarine fans thus must also run out as much as 100's to 1000's kilometers without dissipating or becoming so thick and dilute that they cannot coherently channelize themselves. We refer to such currents as long-runout turbidity currents. Although numerous models of turbidity currents have been presented to date, none has had the capability of satisfying this constraint over such lengths. Here we provide a resolution to this problem.

2. Existing models of turbidity currents

Meiburg & Kneller (2010) presented an overview of both models of turbidity current dynamics and their objectives. Models to date that predict either spatial or spatiotemporal evolution of such currents fall into three classes. The first of these includes layer-averaged models, the second encompasses Reynolds-averaged models that can resolve the structure of the flow in the upward normal direction and averaged flow fields, and the third encompasses high-fidelity (Large Eddy Simulation, LES or Direct Numerical Simulation, DNS) models that resolve all or part of the turbulent structure.

Layer-averaged models for turbidity currents were presented by Fukushima *et al.* (1985) and Parker *et al.* (1986) in the context of submarine canyons. These models are based on an extension of the model of Ellison & Turner (1959) for the downstream evolution of sediment-free dense underflows, such as those driven by thermohaline effects. Ellison & Turner (1959) assumed their ambient fluid to be infinitely deep. This assumption was also used in the formulation of the 3-equation and 4-equation models, and is retained in the analysis below. The models of Fukushima *et al.* (1985) and Parker *et al.* (1986) adapt concepts from Pantin (1979) and Parker (1982) to explain how turbidity currents could "ignite" or self-accelerate via the entrainment of bed sediment. Further developments in layer-averaged modeling have been presented by Garcia (1994), Bonnecaze *et al.* (1993), Fay (2012), Hu *et al.* (2012, 2015), Cao *et al.* (2015), Bolla Pittaluga *et al.* (2018) and Skevington & Dorrell (2024).

The 3-equation and 4-equation layer-averaged models of Fukushima *et al.* (1985) and Parker *et al.* (1986) have been used to study the formation of sediment waves and submarine gullies on the seafloor (Izumi 2004), and cyclic step instability within the flow (Kostic & Parker 2006; Wu & Izumi 2022). A 2D extension of variants of these models have been used to explain incipient self-channelization of turbidity currents via levee emplacement (Imran *et al.* 1998; Halsey & Kumar 2019). Wahab *et al.* (2022) have applied the 4-equation model to the morphodynamics of submarine fans. Traer *et al.* (2018*a*,*b*) have used a version of the 4-equation model to study flow stripping over levees. A version of the model was further developed to simulate the excavation of submarine canyons (Zhang *et al.* 2017).

Reynolds-averaged models of turbidity current dynamics which can resolve the vertical structure of the flow, and in particular $k-\epsilon$ models, have been presented by Eidsvik & Brørs (1989), Sequeiros *et al.* (2009), Yeh *et al.* (2013), Luchi *et al.* (2018) and Iwasaki & Parker (2020). High-fidelity models have been presented by Cantero *et al.* (2009*a*,*b*), Biegert *et al.* (2017), Salinas *et al.* (2019*a*,*b*, 2020, 2021*a*, 2022) and Xie *et al.* (2023*b*).

These different modeling approaches, each of which has its intrinsic value, cannot be used to directly predict long-runout turbidity currents over 100's to 1000's of km. This is either due to computational limitations (for example, DNS) or the configuration studied (for example, lock exchange). The layer-averaged models (e.g. Bolla Pittaluga *et al.* 2018; Skevington & Dorrell 2024) must adopt a mechanism of the flow stripping over preexisting levees to overcome the overthickening problem in order to capture the long-runout feature, which precludes the possibility of using the same model to study the levee formation process (such as Imran *et al.* 1998; Halsey & Kumar 2019).

The Reynolds-averaged model of Luchi *et al.* (2018) and the high-fidelity model of Salinas *et al.* (2021*b*) applied to the Froude-subcritical regime have demonstrated that flow conditions exist which would facilitate long-runout turbidity currents, the former due to flow detrainment and the latter through suppression of turbulence. However, none of these Reynolds-averaged, DNS, and LES models can predict the evolution of the current over hundreds to thousands of kilometers, as such simulations require large computational domains that are computationally prohibitive. Traditional layer-averaged models based on 3-equation and 4-equation models do not present such computational difficulty. They nevertheless suffer from a deficiency in the formulation itself, as illustrated below.

2.1. *Deficiency of layer-averaged approaches to turbidity currents*

The deficiency in question is common to both the 3-equation and 4-equation models of Parker *et al.* (1986), so only the 3-equation model is outlined here. The configuration is shown in figure 3a. The turbidity current is contained within a single layer. It runs over a bed with slope S, has thickness δ and layer-averaged stream velocity U. It carries a dilute suspension of sediment with layer-averaged volumetric concentration C ($C << 1$). The sediment has submerged specific gravity R (where $R = 1.65$ for quartz in water). Where t and x denote time and the down-channel coordinate and g denotes gravitational acceleration, the governing equations for momentum, fluid mass and suspended sediment conservation are

$$\frac{\partial \delta U}{\partial t} + \frac{\partial \delta U^2}{\partial x} = -\frac{1}{2} Rg \frac{\partial C\delta^2}{\partial x} + RgC\delta S - C_{fb}U^2 \tag{2.1}$$

$$\frac{\partial \delta}{\partial t} + \frac{\partial U\delta}{\partial x} = e_{ws}U \tag{2.2}$$

$$\frac{\partial C\delta}{\partial t} + \frac{\partial UC\delta}{\partial x} = v_s\left(E_s - rC\right) \tag{2.3}$$

where C_{fb} is a dimensionless coefficient of bed friction, here taken as constant for simplicity, e_{ws} is a coefficient of water entrainment across the interface between the turbidity current and the ambient fluid, v_s is the fall velocity of sediment, E_s is a dimensionless coefficient of sediment entrainment from the bed into suspension, which is in turn a function of near-bed flow, and r is the ratio of near-bed concentration to layer-averaged concentration. The closure relation for e_{ws} has been empirically obtained as follows (Parker *et al.* 1987)

$$e_{ws} = e_{ws}[Ri_b] = \frac{0.075}{\sqrt{1 + 718 Ri_b^{2.4}}} \tag{2.4}$$

$$Ri_b = \frac{RgC\delta}{U^2} = \frac{Rgq_s}{U^3} \tag{2.5}$$

$$q_s = U\delta C \tag{2.6}$$

Here R_{ib} is a bulk Richardson number and q_s is the volume transport rate of suspended sediment per unit width $[L^2T^{-1}]$. In the case of steady flows that develop spatially downstream, equations (2.1, 2.2, 2.3) can be cast in the forms

$$\frac{\delta}{U}\frac{dU}{dx} = \frac{-\left(1 + \frac{1}{2}Ri_b\right) e_{ws} + Ri_b S - C_{fb} - \frac{1}{2}\frac{v_s}{U} r\, Ri_b \left(\frac{q_{se}}{q_s} - 1\right)}{(1 - Ri_b)} \tag{2.7}$$

$$\frac{d\delta}{dx} = \frac{\left(2 - \frac{1}{2}Ri_b\right) e_{ws} - Ri_b S + C_{fb} + \frac{1}{2}\frac{v_s}{U} r\, Ri_b \left(\frac{q_{se}}{q_s} - 1\right)}{(1 - Ri_b)} \tag{2.8}$$

$$\frac{\delta}{q_s}\frac{dq_s}{dx} = \frac{v_s}{U} r \left(\frac{q_{se}}{q_s} - 1\right) \tag{2.9}$$

where q_{se} is the value of q_s that would be in equilibrium with the local flow;

$$q_{se} = U\delta \frac{E_s}{r} \tag{2.10}$$

The densimetric Froude number of the flow Fr_{db} can be defined as

$$Fr_{db} = \frac{U}{\sqrt{RgC\delta}} = \frac{U^{3/2}}{\sqrt{Rgq_s}} = Ri_b^{-1/2} \tag{2.11}$$

In the case of Froude-supercritical flow ($Fr_{db} > 1; Ri_b < 1$), equations (2.7, 2.8, 2.9) can be integrated downstream upon specification of upstream values U, δ and q_s. As noted above, these relations can be used to predict self-acceleration upon the assumption of appropriate functional forms for E_s and r. The major deficiency of this model is, however, best seen in case of bypass flow, according to which there is no net exchange of sediment with the bed:

$$q_s = const. \quad (e.g. = q_{se}) \tag{2.12}$$

Such flows can be realized, for example, by running the currents over a sediment-starved bed.

The above equations possess a normal flow solution over a constant bed slope S (in the sense of Ellison & Turner 1959) for bypass flow, such that Richardson number Ri_b and velocity U attains a constant value and thickness δ increases linearly with distance downstream:

$$-\left(1 + \frac{1}{2}Ri_b\right) e_{ws}[Ri_b] + Ri_b S - C_{fb} = 0 \tag{2.13}$$

$$\frac{d\delta}{dx} = e_{ws}[Ri_b] \tag{2.14}$$

For given values of S and C_{fb}, (2.13) can be solved in conjunction with (2.4) to obtain the normal flow Richardson number Ri_{bn}, from which normal velocity U_n is found to be

$$U_n = \left(\frac{Rgq_s}{Ri_{bn}} \right)^{1/3} \tag{2.15}$$

The defect associated with these models becomes apparent upon consideration of (2.14). For example, we consider a value of Ri_{bn} of 0.7. This corresponds to a Froude-supercritical flow in the sense that the densimetric Froude number Fr_{db} takes the value $1.20 > 1$. According to (2.4), e_{ws} takes the constant value 0.0043. A current that is 5 m thick upstream ($x = 0$) and has the normal velocity at that point would attain a thickness of at least 1720 m at $x = 400$ km. The suspended sediment concentration at $x = 400$ km would be an order of 10^{-3} times smaller than its upstream value. According to Jobe *et al.* (2020), channels on the Amazon Submarine Fan have bankfull depths ranging from 147 m to 10 m downfan. As noted above in the context of figure 2, the channel is at least 760 km long. Similarly, the channel of the Congo Fan has a depth of about 100-150 m for the first 900 km of the channel (Hasenhündl *et al.* 2024). Referring to the example with $Ri_b = 0.7$, there is no obvious way for 1720 m thick turbidity current, with a suspended sediment concentration that is on the order of one thousandth of its upstream value, to follow a channel that is 10-150 m deep, much less construct it.

The models of Bolla Pittaluga *et al.* (2018) and Skevington & Dorrell (2024) suffer from the same defect of overthickening; the former paper uses the fluid entrainment relation (2.4) from Parker *et al.* (1987), and the latter paper use the similar relation of Parker *et al.* (1986). They achieve long-runout only by limiting current thickness by means of overflow across preexisting levees. Were the levees not already confining the flow, the flow would overthicken and the suspended sediment concentration would become dilute to the point where the flow would be incapable of constructing them.

Cao *et al.* (2015) have succeeded in running a layer-averaged model of turbidity currents in a reservoir over 60 km. Their innovative model is able to capture the plunge point where the river dives into the reservoir to form a bottom turbidity current. During turbidity current events they studied, the deepest part of the reservoir is about 60 m, or around three times the thickness of the turbidity currents. Due to the shallow environment, Cao *et al.* (2015) added a dynamic formulation of the flow in the ambient water above the current as well as the current itself, calling their formulation a “double layer-averaged model”. The volume sediment concentration in the current is around 0.085, corresponding to a hyperconcentrated flow. This and the relatively slow-moving flow dictate value of Ri_b on the order of 100’s, in which case values of e_{ws} are so small that thickening over 60 km is negligible. This result, however, cannot be used to formulate a general model of long-runout turbidity currents because such large bulk Richardson numbers with near-vanishing entrainment of ambient water constitute a special case.

Their model includes a turbidity current layer and an ambient water layer, the dynamics of which must be considered in the shallow setting of the reservoir they model. In that sense, our model is a ”three layer model”: driving layer, driven layer and ambient layer. In our model, we take the ambient water to be infinitely deep, and so can treat it as stagnant, which enables the description of the deep sea environment.

Here we seek a model that allows long-runout turbidity currents over 100’s to 1000’s of kilometers for arbitrary values of Richardson number, which neither overthicken nor become overdilute, and as such would be competent to emplace their own levees far downstream (see Imran *et al.* 1998; Halsey & Kumar 2019).

2.2. *Water detrainment from turbidity currents*

An examination of the above calculations reveals that in the case of bypass conditions, when sediment fall velocity v_s is neglected in the problem, the formulation becomes identical to that of Ellison & Turner (1959) for a conservative contaminant such as dissolved salt. Yet fall velocity should play a role even in bypass suspensions. An easy way to see this is in terms of the Rouse solution for the equilibrium (bypass) vertical distribution of suspended sediment in an open channel. Even though there is no net bed erosion or deposition, the higher the fall velocity, the more the suspended sediment profile is biased toward the bed. Such grain size bias is also observed in direct measurements of turbidity currents and their deposits in the Monterey Canyon (Symons *et al.* 2017), and is built into, for example, the high-fidelity calculations reported in Balachandar *et al.* (2024).

Further insight into the role of sediment fall velocity can be gained by the study of turbidity currents entering into bowl-like basins with horizontal scales on the order of 10's of kilometers, called mini-basins. These basins can fill over time due to the delivery of sediment from turbidity currents (Lamb *et al.* 2004). In the course of experiments on turbidity currents flowing into minibasins, Lamb *et al.* (2006) and Toniolo *et al.* (2006*a*,*b*) recognized a phenomenon they called detrainment. Under the right circumstances, a fully turbulent turbidity current can flow continuously into a minibasin, yet no sediment escapes over the downstream lip of the minibasin. In other words, the turbidity current can form a relatively stagnant pond with a settling interface that equilibrates below the downstream lip of the minibasin. If the pond is sufficiently stagnant, so that there is negligible flow circulation within it (Reece *et al.* 2024), water detrains across the interface and then escapes the minibasin at the rate $v_s A$, where A is the surface area of the settling interface within the minibasin.

With the above in mind, Toniolo *et al.* (2006*b*) proposed a formulation according to which (2.2) is amended to

$$\frac{\partial \delta}{\partial t} + \frac{\partial U\delta}{\partial x} = e_{ws}U - v_s \tag{2.16}$$

In simple terms the fall velocity in (2.16) indicates that the sediment "fights back" against turbulent entrainment into the ambient fluid above. Bolla Pittaluga *et al.* (2018) incorporated this formulation into the 3-equation model.

Luchi *et al.* (2018) further developed this idea using a $k - \epsilon$ model of turbidity currents that naturally accounts for the effect of fall velocity through its presence in the equation of conservation of suspended sediment. Luchi *et al.* (2018) modeled the evolution of the flow down a slope that is uniform in space but developing in time. After a sufficient amount of time, the flow segregates into two layers. The turbulent flow in the bottom layer contains nearly all the suspended sediment, and eventually achieves a near steady-state thickness and streamwise velocity profile. The flow in the top layer is also turbulent but nearly sediment-free, and thickens monotonically in time. They referred to the bottom layer as the "driving" layer, in that the suspended sediment sequestered there provides the impelling force for the flow. They referred to the top layer as the "driven" layer, in that the nearly sediment-free water there is more or less simply dragged along by the driving layer, as in the case of a flow above a plate moving at constant velocity.

The interface between the driving layer and the driven layer in the model of Luchi *et al.* (2018) corresponds to a settling interface. This interface is not necessarily as sharp as that seen in a fully ponded minibasin, because the downward tendency of the settling interface works against turbulent mixing of the flow itself. This notwithstanding, as the driven layer thickens, the mean concentration of suspended sediment in it becomes negligible compared to the driving layer.

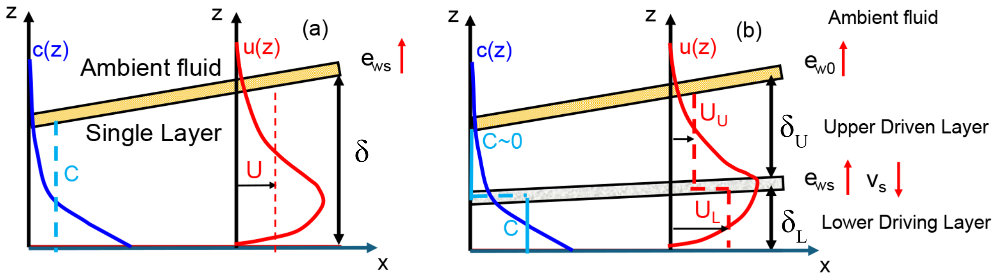

Figure 3: Definition diagram for layer-averaged turbidity currents. (a) Single layer formulation such as used in the 3-equation model; (b) two-layer formulation proposed here.

3. A two-layer formulation

The $k-\epsilon$ model of Luchi *et al.* (2018) is not easily implemented on a scale of 100's or 1000's of kilometers. The essence of the model results can, however, be cast in terms of a much simpler two-layer, layer-averaged model which does have that capability. This configuration is summarized in figure 3b.

The fluid mechanical basis for the two-layer model presented here is the two-layer formulation of Arita & Jirka (1987*a*,*b*) originally designed for the treatment of saline wedges (Several misprints were corrected in Arita 1998). That framework is adapted here, but the characterization of the boundary between the two layers is amended in terms of a settling interface. We also replace the relation for water entrainment used by Arita & Jirka (1987*b*) for saline wedges to (2.4) (Parker *et al.* 1987), which is more appropriate for density underflows.

Let δ_L and δ_U denote the thicknesses of the lower (driving) layer and upper (driven) layer in figure 3b. The corresponding layer-averaged velocities are U_L and U_U. The layer-averaged volume suspended sediment concentration in the lower layer is C; the upper layer is approximated as sediment-free. The friction coefficient at the interface between the two layers is denoted as C_{fi}. The coefficient of water entrainment across the interface between the lower and upper layer is denoted as e_{ws}, whereas the corresponding coefficient between the upper layer and the ambient water is denoted as e_{wo}. In so far as the upper layer is (to a first approximation) sediment-free, the value of e_{wo} can be computed from (2.4) as the limiting value in the absence of stratification ($Ri_b \to 0$), so that $e_{wo} \to 0.075$.

The governing equations for the lower layer are:

$$\frac{\partial U_L\delta_L}{\partial t}+\frac{\partial U_L^2\delta_L}{\partial x} = -\frac{1}{2}Rg\frac{\partial C\delta_L^2}{\partial x} + RgC\delta_L S - C_{fb}U_L^2 - C_{fi}\left|U_L-U_U\right|\left(U_L-U_U\right) \qquad (3.1)$$

$$\frac{\partial \delta_L}{\partial t}+\frac{\partial U_L\delta_L}{\partial x} = e_{ws}\left(U_L-U_U\right) - v_s \qquad (3.2)$$

$$\frac{\partial C\delta_L}{\partial t}+\frac{\partial U_L C\delta_L}{\partial x} = v_s\left[E_s - rC\right] \qquad (3.3)$$

A derivation of (3.2) from the 2D (streamwise – upward normal) continuity equation is provided in the supplementary material. In the case of bypass flows, (3.3) is replaced by (2.12). As opposed to the 3-equation model of Parker *et al.* (1986), however, the effect of sediment does not vanish in the bypass case; it enters through the right-hand side of (3.2). The corresponding forms for the upper layer are

$$\frac{\partial U_U \delta_U}{\partial t} + \frac{\partial U_U^2 \delta_U}{\partial x} = C_{fi}|U_L - U_U|(U_L - U_U) \tag{3.4}$$

$$\frac{\partial \delta_U}{\partial t} + \frac{\partial U_U \delta_U}{\partial x} = e_{wo} U_U - e_{ws}\,(U_L - U_U) + v_s \tag{3.5}$$

Arita & Jirka (1987*b*) evaluate the interfacial friction coefficient as $C_{fi} = 2e_{ws}$. The Richardson number used in (2.4) to compute the turbulent entrainment coefficient e_{ws} must be modified for the two-layer flow, as it is the difference between the velocities U_L–U_U, not U_L itself, that drives entrainment. We thus amend the formulation to

$$e_{ws} = \frac{0.075}{\sqrt{1 + 718 Ri_I^{2.4}}}, \tag{3.6a}$$

$$Ri_I = \frac{RgC\delta}{(U_L - U_U)^2} = \frac{Rgq_s}{U_L(U_L - U_U)^2} \tag{3.6b}$$

which is used to obtain numerical results of the two-layer model.

To illustrate how the two-layer formulation overcomes the shortcomings of the 3-equation model, it is useful to cast equations (3.1 to 3.5) into the form for steady, gradually varied flow corresponding to (2.7 to 2.9). The relations for the lower layer are

$$\begin{aligned}\frac{\delta_L}{U_L}\frac{dU_L}{dx} = \frac{1}{(1-Ri)}\Bigg[&-\left(1+\frac{1}{2}Ri\right)e_{ws}\frac{(U_L-U_U)}{U_L} + \left(1+\frac{1}{2}Ri\right)\frac{v_s}{U_L}\\ &+RiS - C_{fb} - C_{fi}\frac{|U_L-U_U|(U_L-U_U)}{U_L^2} - \frac{1}{2}\frac{v_s}{U_L}rRi\left(\frac{q_{se}}{q_s}-1\right)\Bigg]\end{aligned} \tag{3.7a}$$

$$\begin{aligned}\frac{d\delta_L}{dx} = \frac{1}{(1-Ri)}\Bigg[&\left(2-\frac{1}{2}Ri\right)e_{ws}\frac{(U_L-U_U)}{U_L} - \left(2-\frac{1}{2}Ri\right)\frac{v_s}{U_L}\\ &-RiS + C_{fb} + C_{fi}\frac{|U_L-U_U|(U_L-U_U)}{U_L^2} + \frac{1}{2}\frac{v_s}{U_L}rRi\left(\frac{q_{se}}{q_s}-1\right)\Bigg]\end{aligned} \tag{3.7b}$$

$$\frac{\delta}{q_s}\frac{dq_s}{dx} = \frac{v_s}{U_L}r\left(\frac{q_{se}}{q_s}-1\right). \tag{3.7c}$$

In (3.7a) and (3.7b), Ri is a bulk Richardson number based on the lower layer

$$Ri = \frac{RgC\delta_L}{U_L^2} = \frac{Rgq_s}{U_L^3}. \tag{3.8}$$

The corresponding equations for the upper layer are

$$\frac{\delta_U}{U_U}\frac{dU_U}{dx} = -e_{wo} + e_{ws}\frac{(U_L-U_U)}{U_U} - \frac{v_s}{U_U} + \frac{C_{fi}|U_L-U_U|(U_L-U_U)}{U_U^2}, \tag{3.9a}$$

$$\frac{d\delta_U}{dx} = 2e_{wo} - 2e_{ws}\frac{(U_L-U_U)}{U_U} + 2\frac{v_s}{U_U} - \frac{C_{fi}|U_L-U_U|(U_L-U_U)}{U_U^2}. \tag{3.9b}$$

As in the case of the single layer model, when the flow in the lower layer is Froude supercritical, i.e. ($Ri < 1$), the above equations can be integrated downstream from specified upstream values of U_L, δ_L, q_s, U_U and δ_U.

3.1. *Normal flow for bypass conditions*

To show how the introduction of settling detrainment affects the behavior of a turbidity current, we consider the case of bypass flow, so that (3.7c) is replaced with (2.12). Accordingly, (3.7a) and (3.7b) reduce to

$$\frac{\delta_L}{U_L}\frac{dU_L}{dx} = \frac{1}{(1-Ri)}\left[-\left(1+\frac{1}{2}Ri\right)e_{ws}\frac{(U_L-U_U)}{U_L} + \left(1+\frac{1}{2}Ri\right)\frac{v_s}{U_L} + RiS - C_{fb} - C_{fi}\frac{|U_L-U_U|(U_L-U_U)}{U_L^2}\right] \tag{3.10a}$$

$$\frac{d\delta_L}{dx} = \frac{1}{(1-Ri)}\left[\left(2-\frac{1}{2}Ri\right)e_{ws}\frac{(U_L-U_U)}{U_L} - \left(2-\frac{1}{2}Ri\right)\frac{v_s}{U_L} - RiS + C_{fb} + C_{fi}\frac{|U_L-U_U|(U_L-U_U)}{U_L^2}\right] \tag{3.10b}$$

Just as in the case of the 3-equation bypass model and Ellison & Turner (1959), these equations have a normal flow solution. Setting $dU_L/dx = 0$ in (3.10a) and $dU_U/dx = 0$ in (3.9a), it is possible to solve for the constant normal values U_{Ln} and U_{Un}. From these values, it can be found that (3.10b) and (3.9b) reduce to the forms

$$\frac{d\delta_L}{dx} = A_L \tag{3.11a}$$

$$\frac{d\delta_U}{dx} = A_U \tag{3.11b}$$

where A_L and A_U are constants obtained from the right-hand sides of (3.10b) and (3.9b). In summary, at normal flow, the velocities of both the lower and upper layers are constant, and the layer thicknesses of the lower and upper layers increase linearly downstream. We find below that the effect of settling renders the downstream growth rate of the lower layer much less than the upper layer, indeed so much less that a turbidity current is likely able to track (and thus potentially make) its own channel.

The relations for U_{Ln} and U_{Un} can be cast in dimensionless form as follows; where

$$Ri_n = \frac{Rgq_s}{U_{Ln}^3}, \quad Ri_{In} = \frac{Rgq_s}{U_{Ln}^3(1-\Gamma)^2}, \quad \Gamma = \frac{U_{Un}}{U_{Ln}}, \quad \tilde{v}_s = \frac{v_s}{(Rgq_s)^{1/3}} \tag{3.12a-d}$$

we obtain

$$\left(1+\frac{1}{2}Ri_n\right)\left[\tilde{v}_s Ri_n^{1/3} - e_{ws}\left[Ri_{In}\right](1-\Gamma)\right] + Ri_n S - C_{fb} - 2e_{ws}[Ri_{In}](1-\Gamma)^2 = 0 \quad , \tag{3.13a}$$

$$-e_{wo}\Gamma^2 + e_{ws}\left[Ri_{In}\right]\Gamma(1-\Gamma) - \tilde{v}_s Ri^{1/3}\Gamma + 2e_{ws}\left[Ri_{In}\right](1-\Gamma)^2 = 0. \tag{3.13b}$$

From (3.13a,b), it can be found that once the three parameters S, $\tilde{v}_s$ and C_{fb} are specified, the two variables Ri_n and Γ can be determined. These values in turn set the dimensional values U_U and U_L. Thus U_U and U_L at the normal flow condition do not depend on boundary conditions. Here, without losing generality, we set $C_{fb} = 0.002$ which is typical for fine-grained channels (Konsoer *et al.* 2013; Ma *et al.* 2017, 2020; Simmons *et al.* 2020). A wide range of values S and $\tilde{v}_s$ compatible with submarine channels (Covault *et al.* 2011), are chosen to illustrate solutions to the normal flow condition obtained from solving (3.13a,b).

The results are shown in figures 4a-d. The pattern of normal flow solutions divides in to a Froude-supercritical regime defined in terms of the lower layer ($Ri < 1$) for sufficiently large values of S and $\tilde{v}_s$, and a Froude-subcritical regime ($Ri > 1$) as S and $\tilde{v}_s$ become small. A clear threshold behavior can be identified: when $S > 0.0063$ or $\tilde{v}_s > 0.0042$, the flow is always Froude-supercritical regardless of the value of the other parameter. Assuming $q_s = 0.6$ m^2/s (a value justified below) as an example in the computation of $\tilde{v}_s$, three lines corresponding to grain sizes D =31.25, 62.5, 125 μm (specific gravity of quartz so R = 1.65 and water temperature = 20°C) are plotted on all four panels.

3.2. *Calculations at field scale under bypass conditions*

Advances in field measurements have shown that turbidity currents come in a variety of shapes and sizes (Xu *et al.* 2004; Dorrell *et al.* 2014; Hughes Clarke 2016; Paull *et al.* 2018; Talling *et al.* 2022; Pope *et al.* 2022), mainly depending on the size of the systems and the transported grain sizes. Long-runout flows are known to have emanated from the Gaoping Canyon and the Grand Banks Canyon, where breakages of submarine telecommunication cables have provided indications of peak velocities around 15-20 m/s (Hsu *et al.* 2008; Heezen & Ewing 1952). More recently, measurements of long-runout flows have been made in the Congo Canyon, where flows can accelerate for over 1200 km to reach peak velocities of 8 m/s upon reaching the abyssal plain at a water depth of over 5 km (Talling *et al.* 2022). Unfortunately, this flow was so powerful that it destroyed all the instrumentation, and consequently there are no flow discharge measurements from this event. More detailed velocity measurements of smaller flows in the Congo Canyon show that at ~150 km offshore and a water depth of almost 2 km, turbidity current events have peak discharges of up to ~16 000 m^3/s and typically last for about a week (Azpiroz-Zabala *et al.* 2017). Following the passage of the faster head of the flow, a flow speed of about 0.75 m/s is typically maintained for 5 days, but occasionally for up to 8 days (Simmons *et al.* 2020). However, these detailed measurements are unlikely to be channel-forming turbidity currents. For the rarer and more powerful channel-forming flows, we refer to the reconstruction of channel-forming turbidity currents by Konsoer *et al.* (2013).

Konsoer *et al.* (2013) reconstructed channel-forming flows in turbidity currents by means of an approximate matching of current driving force with rivers. They offer two estimates each for mean sediment concentration C and the bed resistance C_{bf}. Of these, we choose C_u = 0.006 and C_{bf} = 0.002 where C_u is the upstream boundary condition for C. The levee-to-levee channel width of the Amazon Submarine Channel at x = 270 km is found to be about 2 km in figure 3d of Pirmez & Imran (2003). The channel-forming discharge at this width can be estimated to be 200 000 m^3/s according to figure 9 of Konsoer *et al.* (2013). Therefore, we assume a water discharge per unit width q_{wu} at the upstream end of our calculation of 100 m^2/s. In so far as we consider bypass currents, we hold the volume sediment discharge per unit width q_s at the constant value 100 m^2/s × 0.006 = 0.6 m^2/s. This is the justification for using q_s = 0.6 m^2/s in figure 4.

We now show numerical results for the spatial, down-canyon development of a bypass turbidity current. All the calculations shown below assume a size of 62.5 μm for the suspended sediment, a bed friction coefficient C_{fb} = 0.002, a suspended sediment transport rate per unit width of 0.6 m^2/s, an upstream flow discharge q_{wu} of 100 m^2/s and an upstream volume suspended sediment concentration C_u of 0.006. We consider two cases for slope: one with a constant slope of 0.03, and one with a slope that exponentially declines downstream in approximate concordance with the long profile of figure 2b. The numerical results were obtained by solving equations (3.10a,b) and (3.9a,b). The cases below are for the Froude-supercritical condition, which allows a stepwise downstream numerical solution to (3.9)

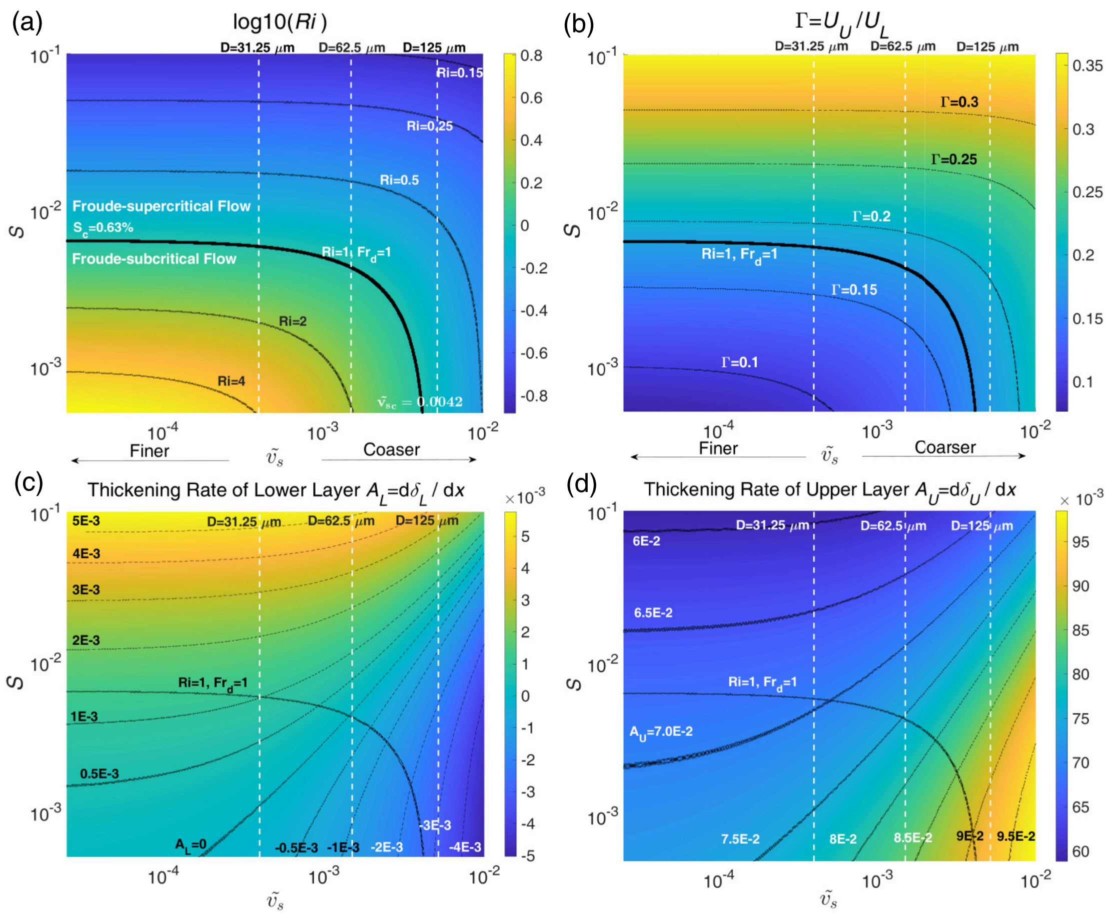

Figure 4: Bulk Richardson number of the lower layer Ri and the velocity ratio Γ of U_U to U_L solved from equations (3.13a,b) for various combinations of channel slope S and dimensionless settling velocity $\tilde{v_s}$ at bypass normal flow. (a) Ri as a function of S and $\tilde{v_s}$. Since the lower-layer Froude number $Fr_d = 1/\sqrt{Ri}$, the isoline $Ri = 1$ separates the Froude super- and sub-critical flow regimes. A clear threshold behavior can be identified: when $S > 0.0063$ or $\tilde{v_s} > 0.0042$, the flow is always Froude supercritical regardless of the value of the other parameter; (b) $\Gamma = U_{Un}/U_{Ln}$ as a function of S and $\tilde{v_s}$. Note that the upper layer is always slower than the lower layer: this effect strengthens as S and $\tilde{v_s}$ become small; (c) A_L as a function of S and $\tilde{v_s}$. There is a neutral line where water entrainment due to turbulent mixing and water detrainment due to sediment settling zeros out. Below the line where S is small and $\tilde{v_s}$ is large, the turbidity currents may subside (negative thickening rate) due to sediment-settling induced drop in the level of the interface; (d) A_U as a function of S and $\tilde{v_s}$. A_U is at least one order magnitude larger than A_L because the ambient water entrainment coefficient e_{w0}=0.075 sets the top interface boundary condition for the upper layer, which corresponds to the upper bound for this coefficient. Assuming $q_s = 0.6$ m^2/s, three lines corresponding with D=31.25, 62.5, 125 μm are plotted on all figures.

and (3.10). Sample numerical results under a Froude-subcritical condition can be found in supplementary material figure B.1.

Figure 5 shows the downstream development of a bypass flow over a constant slope S of 0.03. This slope has been chosen in so far as it is representative of the constant-slope channel profiles of Covault *et al.* (2011) shown in figure 2a. In figure 5, two Froude-supercritical

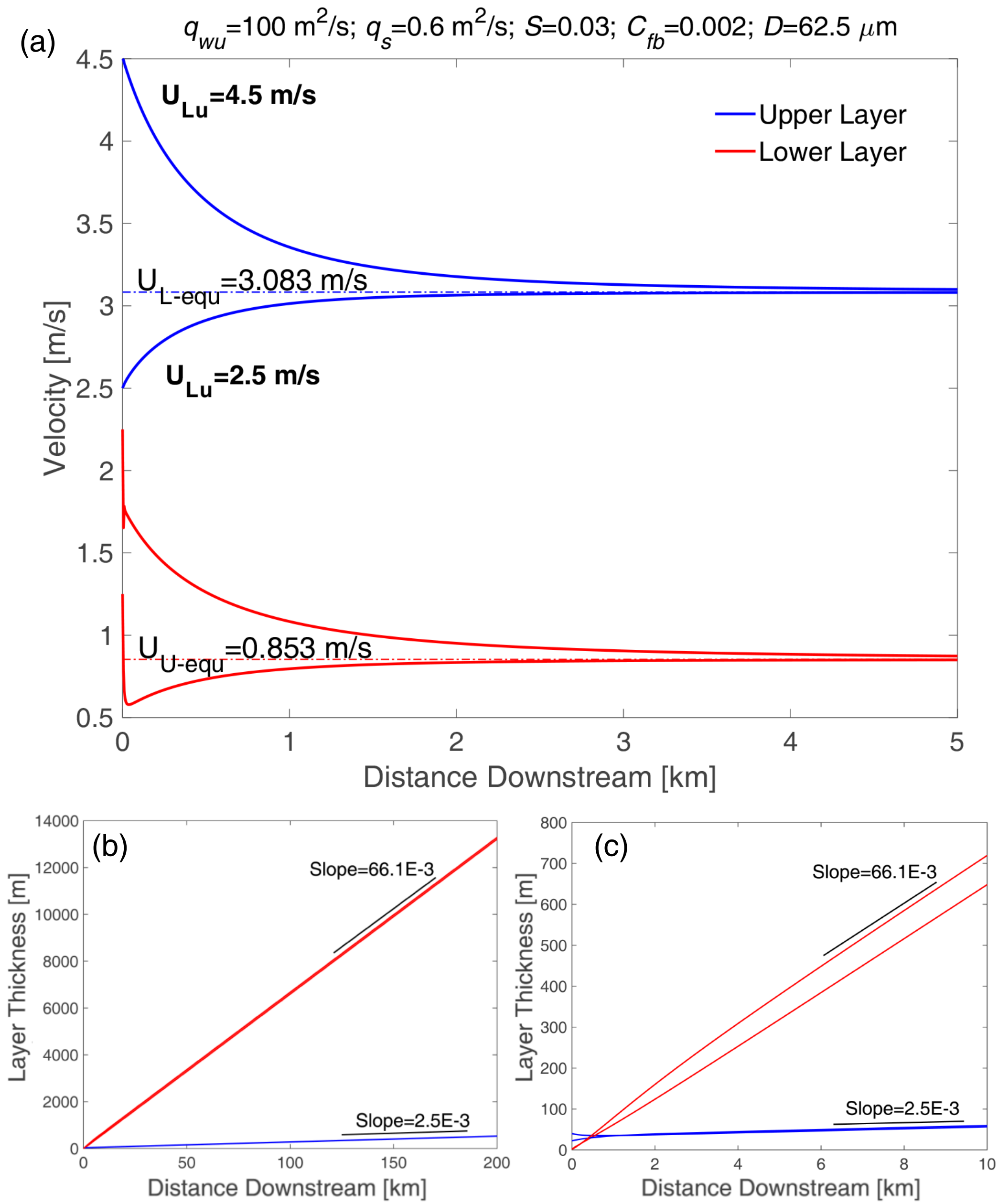

Figure 5: (a) Spatial evolution of the lower layer and upper layer velocities U_L and U_U, over a 5-km reach, starting from two sets of upstream conditions. In all cases the velocities evolve toward normal flow. (b) Spatial evolution of thicknesses of the lower and upper layers δ_L and δ_U over a 200-km reach. (c) Spatial evolution of lower and upper layer thicknesses δ_L and δ_U over a 10-km reach, using two different sets of upstream conditions.

upstream conditions have been chosen for the numerical solution of (3.9a,b) and (3.10a,b): $(U_L, U_U, \delta_L, \delta_U)$ = (2.5 m/s,1.25 m/s, 40 m, 1 m) and (4.5 m/s, 2.25 m/s, 22.22 m, 1 m).

In figure 5a velocities converge to the normal values (U_L, U_U) = (3.083 m/s, 0.853 m/s) within about 5 km. It is not necessary to confirm that these correspond to long-runout values;

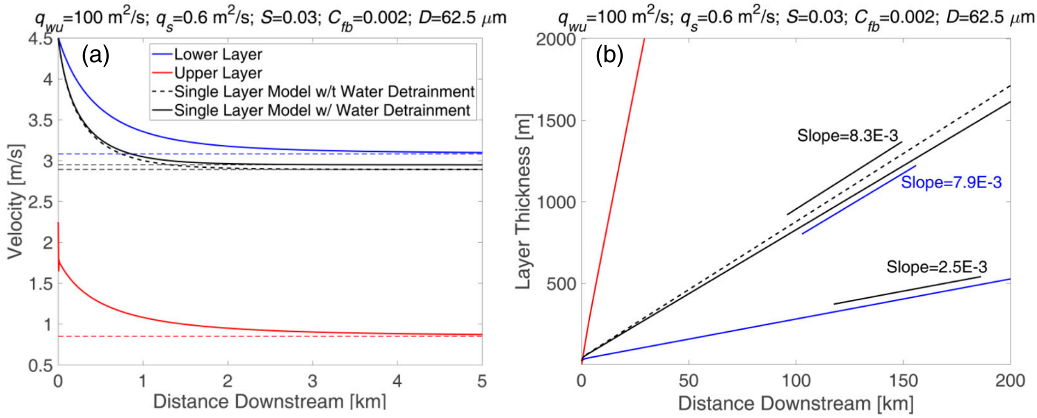

Figure 6: Comparison of spatial development on the slope $S = 0.03$. (a) Spatial evolution over a 5-km reach of lower layer velocity U_L and upper layer velocity U_U of the two-layer model, velocity U of the 3-equation model, and velocity U of the 3-equation model modified to include detrainment; (b) Spatial evolution over a 200-km reach of lower layer thickness δ_L of the two-layer model, thickness δ of the 3-equation model, and thickness δ of the 3-equation model modified to include detrainment.

on a constant slope, they would not change even 100's of kilometers downslope. The result $U_L < U_U$ confirms that the lower layer is the driving layer, and the upper layer is the driven layer.

Figure 5b shows the development of the layer thicknesses δ_L and δ_U out to 200 km. By 200 km δ_U has thickened to over 13 000 m, an unreasonable value in line with the overthickening of the original 3-equation model. This issue is considered in more detail in the Discussion. The lower layer, on the other hand, has thickened to only 520 m. This is comparable with a channel depth of 165 m, and a levee crest to back-levee elevation difference of at least 270 m at the Shepard Bend of Monterey Channel (Fildani *et al.* 2006), which is about 140 km downchannel of the canyon head. This system has a mean down-channel slope close to the value of 0.03 assumed here (Covault *et al.* 2011). Figure 5c is identical to figure 5b except that the spatial domain has been reduced to 10 km. The results clearly show that in the two-layer model, the lower layer thickens downstream at a much slower rate (factor of 0.038) than the upper layer, whereas the upper layer thickens at a rate higher than that predicted by the single layer 3-equation model.

Figure 6 provides a comparison of the spatial evolution predicted by three models: the two-layer model described here (equations 3.9a,b and 3.10a,b), the original 3-equation model (equations 2.1, 2.2 and 2.12) (Fukushima *et al.* 1985; Parker *et al.* 1986) and the 3-equation model modified to include detrainment (equations 2.1, 2.16 and 2.3) (Toniolo *et al.* 2006*a*; Bolla Pittaluga *et al.* 2018). Again the bed slope S is held constant at 0.03. All calculations use one of the sets of upstream conditions of figure 5. Figure 6a shows spatial evolution of velocity over a 5-km reach. The results for U_L of the two-layer model, U of the 3-equation model and U of the 3-equation model modified to include detrainment all show similar spatial evolution, and approach nearly the same normal velocity. Figure 6b shows spatial evolution over a 200-km reach of δ_L of the two-layer model, δ of the 3-equation model and δ of the 3-equation model modified to include detrainment. The predictions for δ from both versions of the 3-equation model at 200 km are greatly in excess of that predicted for δ_L by the two-layer model. In figure 7, a current running down a long, concave upward profile is considered. Slope declines downstream in accordance with an exponential law that is an approximate fit to figure 2b (Amazon submarine channel) over 800 km:

$$S = S_u e^{-(x/x_e)} \tag{3.14}$$

where x and x_e are in km, x_e= 265.8 km and S_u = 0.0166.

Figure 7a shows the downstream evolution over a 400 km reach of U_L and U_U of the two layer model, and U of the original 3-equation model and the version modified for detrainment. We terminate the calculation where the Froude number declines to the Froude-critical value ($Fr_d = 1$); a hydraulic jump may occur upstream of this point depending on downslope conditions. It can be seen that both versions of the 3-equation model reach the condition $Fr_d = 1$ at distances shorter than 400 km. The two-layer model reaches $Fr_d = 1$ at 402 km. The results for U_L compare well with those for U of the two versions of the 3-equation model, with values declining to 2.14 m/s at x = 400 km. The predicted values of U_U are uniformly lower than U_L, again indicating that the upper layer is driven by the lower layer. Also shown in the diagram is the slope profile; S = 0.0037 at x = 400 km. Figure 7b shows the corresponding results for δ_L,and δ_U and also δ predicted by the two versions of the 3-equation model. The predicted values of δ of the 3-equation models are far too high to follow any channel so far down the system. The predicted value of δ_L, on the other hand, is at 250 m at x = 200 km, a value that compares reasonably with estimates of channel bankfull depth (see below) (Pirmez & Imran 2003; Fildani *et al.* 2006).

Figure 7c shows the long profiles of the Froude number $Fr_d (= Ri^{-1/2}))$ predicted for the lower layer of the two-layer model and the two versions of the 3-equation model. Froude number declines downstream toward unity in all three cases. In the case of the 3-equation model, critical flow is attained at x = 260 and 380 km, respectively. In the two-layer model it is attained at x =402 km. As noted above, the implication is that a hydraulic jump may occur somewhat upstream of this point. The spatially varying model encompassed in (3.9a,b) and (3.9a,b) cannot capture hydraulic jumps. A shock-fitting solution to the primitive equations (3.1), (3.2), (3.4) and (3.5) would, however, capture them (Fildani *et al.* 2006).

Figures 7d and 7e respectively show the down-channel evolution of water discharge per unit width q_w and suspended sediment concentration C. Note that q_w reaches a maximum and then declines after x = 328 km, and C reaches a minimum and then increases after this point. These extreme points are because U_L can quickly adjust to the local equilibrium value, which decreases with exponentially declining channel slope. This flow slowdown effect dominates farther downstream, where δ_L increases more slowly than linear. As a result $q_w = U_L \delta_L$ declines downstream of its peak value. Concentration C has a minimum at the same location because $C = q_s/q_w$ and q_s is constant for the bypass condition.

A lower layer thickness δ_L of 250 m at x = 200 km compares well with the observed channel depth of around 110-170m in the Amazon system (Pirmez & Imran 2003). It should be expected that flow thickness exceeds channel depth, but be of the same order of magnitude in order to construct the channel and its levees. The present model is 1D, which means that it corresponds to flow between frictionless vertical walls. In actual submarine channels, flow stripping, i.e. the overflow which builds the levees and confines the channel, should cause streamwise flow discharge to decline downstream. A possible way to incorporate this process into a model of long-runout turbidity currents is presented by Spinewine *et al.* (2011) and later by (Bolla Pittaluga *et al.* 2018; Skevington & Dorrell 2024).

4. Discussion

The two-layer model of bypass turbidity currents presented here offers many avenues for future development, allowing us to extend our understanding of the fluid dynamics and

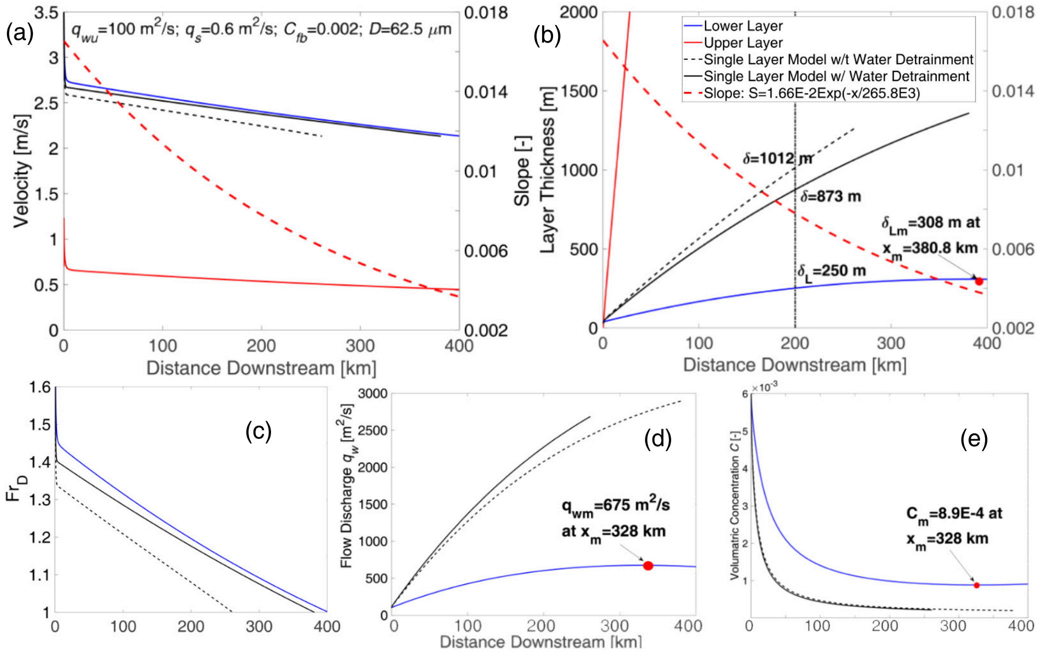

Figure 7: Bypass calculations based on a simplified profile of the Amazon Canyon-Fan system, using 62.5 μm suspended sediment over a 400-km reach. (a) Spatial evolution of velocities U_L and U_U for the two-layer model, U for the 3-equation model, and U for the 3-equation model modified to include detrainment. The slope profile is also shown; (b) Spatial evolution of thicknesses δ_L and δ_U for the two-layer model, δ for the 3-equation model and δ for the 3-equation model modified to include detrainment; (c) Densimetric Froude number Fr_d for the lower layer of the two-layer model, the 3-equation model and the 3-equation model modified to include detrainment; (d) Spatial evolution of water discharge per unit width q_w for the lower layer of the two-layer model, the 3-equation model and the 3-equation model modified to include detrainment; (e) Spatial evolution of the suspended sediment concentration C in the lower layer of the two-layer model, the 3-equation model and the 3-equation model modified to include detrainment.

morphodynamics of long-runout turbidity currents and the morphologies they create. We enumerate a few of these below.

The example flows that are modeled here are limited to steady, Froude-supercritical flows that develop in the downstream direction. By definition, such a steady flow that has run out 1000 km must be continuously occupying the channel for 1000 km. Measurements in the Congo Submarine Channel indicate that turbidity current events can last for a week or more in the proximal part of the system (Azpiroz-Zabala *et al.* 2017) and for up to several weeks in the distal part of the system (Baker *et al.* in review). As the head of the flows outruns the rest of the flow, these flows are likely to stretch to 100's of kilometers long and last for weeks in the distal part of the system. Such stretching flows can be modeled, at least in part, by abandoning the steady, gradually varied flow assumption, and instead solving the full time-varying equations (3.1), (3.2), (3.4) and (3.5), and for bypass flows, (2.12). An appropriate shock-capturing numerical technique such as the one used by Kostic & Parker (2006) and Cao *et al.* (2015) can model unsteady flow whether Froude-supercritical or Froude-subcritical. It was used by Kostic & Parker (2006) to reproduce the migrating turbidity current head and hydraulic jump of one of the experiments of Garcia & Parker (1989). The same formulation could presumably be used to model the hydraulic jumps observed in the field by Sumner *et al.* (2013) and Hughes Clarke (2016).

A bypass current cannot be used directly to model the morphodynamics of bed evolution. Morphodynamics can, however, be modeled by implementing the full forms of (3.1) – (3.5), along with the Exner equation of bed sediment conservation. That is, where η = bed elevation, λ= bed porosity and q_b is the volume rate of bedload transport per unit width:

$$(1-\lambda)\frac{\partial \eta}{\partial t} = -\frac{\partial q_b}{\partial x} + v_s\left(rC - E_s\right). \tag{4.1}$$

Appropriate closure assumptions are necessary for E_s, r and q_b. For example, Parker *et al.* (1987) and Garcia & Parker (1991) present closures for E_s and r, and a closure for q_b that is valid up to and including the regime of unidirectional bedload sheet flow is given in Ribberink (1998). Among the various submarine phenomena that can be revisited with a morphodynamic two-layer formulation are field observations of accelerating flow on constant and decreasing slopes (Talling *et al.* 2022), flows that grow rapidly in sediment volume by a factor 100-1000 (Pope *et al.* 2022; Böttner *et al.* 2024), and the formative conditions for large trains of knickpoints (Heijnen *et al.* 2020) or smaller trains of upstream-migrating crescentic bedforms (Hughes Clarke 2016). A morphodynamic version of the two-layer model can also be adapted to model the incision necessary to excavate submarine canyons (Zhang *et al.* 2017) with the aid of, for example, the sandblasting model of Lamb *et al.* (2008).

The 3- and 4-equation models have, after extension to a 2D streamwise-lateral form, been used to explain self-channelization of turbidity currents via levee emplacement (Imran *et al.* 1998; Halsey & Kumar 2019) and the emplacement of channelized submarine fans (Wahab *et al.* 2022). Due to the limitations of these models, such features have been successfully modeled out to only around 5-25 km. The new two-layer model offers the possibility of modeling levee emplacement over most of the length of a long-runout turbidity current path. Built into such a model would be a characterization of flow stripping (channel overflow; Spinewine *et al.* 2011), which would cause flow discharge to decline downstream and bring the flow thickness more inline with the observed levee elevations.

Field measurements have shown that the dynamics of the migrating front, or nose of a turbidity current may be too complex to be modeled even using a version of the two-layer model that captures front behavior, as sediment concentrations can be above 10% (Paull *et al.* 2018; Wang *et al.* 2020). A first step in overcoming this issue is suggested by the model of Spinewine & Capart (2013) for intense flow and sediment transport at the nose of a dam-break flow. It may be possible to adapt this formulation to the front of a turbidity current otherwise modeled by the present two-layer formulation.

The two-layer model presented here represents an extension of the 3-equation model of Fukushima *et al.* (1985) and Parker *et al.* (1986). Cao *et al.* (2015) referred to their model as a ”double-layer averaged model”. Their model includes a turbidity current layer and an ambient water layer, the dynamics of which must be considered in the shallow setting of the reservoir they model. In that sense, our model is a ”three layer model”: driving layer, driven layer and ambient layer. In our model, we take the ambient water to be infinitely deep, and so can treat it as stagnant, which enables the description of the deep sea environment. Parker *et al.* (1986) also include a 4-equation model, where the extra equation accounts for the balance of turbulent kinetic energy. In principle, the extension of kinetic energy balance to the two-layer model is straightforward, adding one extra equation each to the formulation for the lower and upper layers. It may be useful to revisit the formulation in light of the results of Fay (2012) and Skevington & Dorrell (2024).

Numerical methods that resolve the upward-normal structure of the flow, such as $k-\epsilon$, LES or DNS may not be feasible to implement for long-runout turbidity currents. They nevertheless could be used to develop refined closures for the two-layer model that enhance its performance and accuracy.

While the entrainment coefficient e_{wo} = 0.075 for unstratified turbulent flow is well-justified by data, it may not apply to upper layers that are predicted by the present model to become 1000's of meter thick (for example, as shown in figure 5b above). There are a number of potential reasons why e_{wo} might not attain such a high value. First, a semi-empirical, fully turbulent entrainment coefficient of e_{wo}=0.075 corresponds to the limit of a plane free jet ($Ri \rightarrow 0$; Parker *et al.* 1987). The rate of production of turbulent energy for such a flow should scale as du/dz, where z is the upward normal coordinate and u is local streamwise velocity averaged over turbulence. As the upper layer becomes thicker and thicker, the term du/dz may drop to the point that full turbulence can no longer be maintained. Were an entirely sediment-free upper layer flow to become fully laminar, dU would scale as $x^{1/2}$ at normal flow in accordance with the Prandtl result for laminar flow over a flat plate, rather than the turbulent scaling $dU \sim x^1$ used here. Second, we have adopted a relation between entrainment rate e_{ws} and Richardson number Ri_I at the interface between the lower and upper layers, again assuming fully turbulent flow (Parker 1982; Parker *et al.* 1987; Johnson & Hogg 2013). Especially for flow in the Froude-subcritical range, however, there are conditions under which stratification is so strong at the lower-upper interface that turbulence is extinguished there (Salinas *et al.* 2021*a*). Under such conditions, mixing at both lower-upper and upper-ambient interfaces is likely to be governed by laminar processes, and can thus be expected to be much weaker than that predicted by (3.6). Information in Arita & Jirka (1987*a*) suggests that the condition for the domination of entrainment by laminar effects becomes more stringent with increasing Reynolds number of the lower layer. Third the value e_{wo} = 0.075 is for a 2-dimensional plane jet where the flow is not allowed to spread in the third dimension; however, the upper layer loses confinement and turns 3D when it overspills the submarine levee, reducing the entrainment coefficient (Rajaratnam 1976) and causing direct loss of water, e.g. flow stripping (Fildani *et al.* 2006; Spinewine *et al.* 2011). Moreover, although very dilute, there should still be some sediment in the upper layer entrained from the lower layer which can also reduce entrainment coefficient (Salinas *et al.* 2019*b*). The present model is 1D in nature and cannot capture lateral expansion of both the lower and upper layers, and corresponding effects that would help limit the streamwise increase in flow thickness. The two-layer model may thus merit modifications in light of the above comments.

The two-layer model with a single grain size can be adapted in a straightforward way to a 3-layer model with two grain sizes. Choosing one of these grain sizes to be in the sand range and the other to be in the mud range can help clarify the nature of morphodynamic channel-levee interaction (Deptuck & Sylvester 2017). It can also further quantify the role of mud which has a relatively small settling velocity, in maintaining sand which has a relatively high fall velocity, in suspension, so as to transport the sand farther downstream (Salaheldin *et al.* 2000). More complex grain size distributions and patterns of dispersion can be considered in the future (Xie *et al.* 2023*a*).

5. Conclusions

Turbidity currents are bottom density flows driven by the excess weight of suspended sediment. Turbidity currents in the deep sea are known to sculpt leveed channels that are 100's to 1000's of kilometers long. To construct such channels, a current must run out at least that far, consistently following the channel that is sculpted by the current itself. No existing model of turbidity current dynamics is capable of accomplishing this. Here, informed by the $k-\epsilon$ model of Luchi et al. (2018), we quantify the problem in terms of a simpler two-layer model. The lower (driving) layer is where nearly all suspended sediment is sequestered.

This sediment is assumed to have a single, constant settling velocity and be transported as a dilute suspension. The upper layer is nearly sediment-free, and is dragged along by the lower (driving) layer. It is essential to introduce the concept of detrainment across the two-layer interface to quantify how sediment resists upward turbulent mixing via its fall velocity, an issue that was first systematically studied in the context of turbidity currents entering a minibasin (Toniolo *et al.* 2006*a*). We apply the model to sediment bypass conditions, such that there is no net flux of sediment at the bed. The model presents a normal flow solution analogous to that of Ellison & Turner (1959) for thermohaline bottom density flows. At normal flow, both lower and upper velocities U_L and U_U attain constant values, and both lower and upper layer thicknesses δ_L and δ_U increase linearly downstream. Under normal flow conditions, two thresholds are identified: one related to channel slope and the other to the nondimensional settling velocity. Exceeding either threshold causes the turbidity current to become Froude-supercritical. Although both layers thicken linearly downstream, we show that the effect of detrainment mediated by fall velocity dramatically slows the thickening rate of lower layer. Our calculations using gradually varied flow show that lower layer of a turbidity current can run out 400 km without over-thickening to the point that it would lose track of its own channel. The calculations terminate there only because the flow reaches the Froude-critical condition, beyond which the computational method is no longer applicable. This issue can be overcome in the future by solving the parent unsteady, non-uniform version of the model (equations 3.1-3.5). The model opens up further future avenues in the study of the fluid dynamics and morphodynamics of long-runout turbidity currents, including non-bypass flows, levee construction and the effect multiple sediment sizes on grain size-specific sediment runout.

Funding. H.M. is supported by China's MST Key R&D grant 2023YFC3206204; M.C. is supported by a Royal Society Research Fellowship (DHF\R\231008).

Declaration of interests. The authors report no conflict of interest.

Data availability statement. The data/code that support the findings of this study are available from the corresponding author upon reasonable request.

Author ORCIDs. H. Ma, https://orcid.org/0000-0002-6017-8113; M. Cartigny, https://orcid.org/0000-0001-6446-5577;

Author contributions. G.P. conceived the study, developed the theoretical formulations and led the writing of the first version of the manuscript; H.M. obtained the exact solution and conducted the numerical simulations; E.V. and H.M. verified the formulations and analyses; G.P. M.C. S.B. E.V. and H.M. interpreted the results; all authors contributed to the discussion of the research and to the writing of the manuscript

Appendix A. Derivation of Equation (3.2) of the main text.

The flow is incompressible turbulent, uniform in the transverse direction, and contains a dilute suspension of sediment with fall velocity v_s. It is assumed that the flow velocity averaged over turbulence is (u, w), where u is the velocity in the x direction and w is the velocity in the z direction. The equation of continuity is

$$\frac{\partial u}{\partial x} + \frac{\partial w}{\partial z} = 0 \tag{A 1}$$

The velocity (u_s, w_s) of a sediment particle is taken to be

$$(u_s, w_s) = (u, w - v_s). \tag{A 2}$$

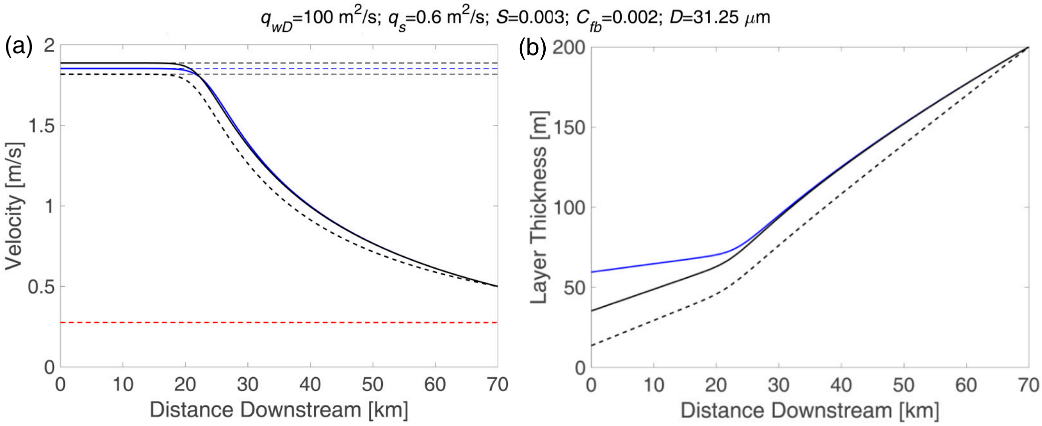

Figure B.1: Numerical results of long profiles of gradually varied flow velocity (a) and layer thickness (b) under Froude-subcritical conditions. The blue line represents the lower layer of the two-layer model. The black dashed line represents the original 3-equation model, and the black solid line represents the 3-equation model with the water detrainment term. The red dashed line represents the upper layer velocity. The solutions were obtained by integrating upstream from the downstream boundary $(U_L, U_U, \delta_L, \delta_U)$ = (0.5 m/s, 0.275 m/s, 200 m, An arbitrary large value) at x = 70 000 m.

Integrating (A 1) from $z = 0$ to $z = \delta_L$ yields

$$\frac{\partial}{\partial x}\int_0^{\delta_L} u dz - u|_L \frac{\partial \delta_L}{\partial x} + w|_{\delta_L} = 0. \tag{A 3}$$

The settling interface is a material interface following the sediment, not the fluid. An appropriate version of the kinematic boundary condition for this case is

$$\frac{\partial \delta_L}{\partial t} + u|_{\delta_L}\frac{\partial \delta_L}{\partial x} - \left(w|_{\delta_L} - v_s\right) = u_e \tag{A 4}$$

where u_e is a turbulent entrainment velocity of fluid across the interface. Set

$$u_e = e_{ws}(U_L - U_U) \tag{A 5}$$

where e_{ws} is a coefficient of turbulent entrainment. Define

$$U_L\delta_L = \int_0^{\delta_L} u dz \tag{A 6}$$

Between (A 3) – (A 6),

$$\frac{\partial \delta_L}{\partial t} + \frac{\partial U_L \delta_L}{\partial x} = e_{ws}(U_L - U_U) - v_s. \tag{A 7}$$

Appendix B. Gradually varied flow under a Froude-subcritical condition

The numerical results under the Froude-subcritical condition are shown in figure B.1. The channel slope is set one order of magnitude smaller than the Froude-supercritical case (figures 5,6) and grain size is halved. Under the Froude-supercritical condition, the boundary condition is given downstream and equations (3.10a,b) and (3.9a,b) are integrated upstream to obtain the numerical results.

REFERENCES

Arita, Masamitsu 1998 *Environment of the Hydrosphere*. Tokyo Denki University Publishing House.

Arita, Masamitsu & Jirka, Gerhard H 1987*a* Two-Layer Model of Saline Wedge. I: Entrainment and Interfacial Friction. *Journal of Hydraulic Engineering* **113** (10), 1229–1246.

Arita, Masamitsu & Jirka, Gerhard H 1987*b* Two-Layer Model of Saline Wedge. II: Prediction of Mean Properties. *Journal of Hydraulic Engineering* **113** (10), 1249–1263.

Azpiroz-Zabala, Maria, Cartigny, Matthieu JB, Talling, Peter J, Parsons, Daniel R, Sumner, Esther J, Clare, Michael A, Simmons, Stephen M, Cooper, Cortis & Pope, Ed L 2017 Newly recognized turbidity current structure can explain prolonged flushing of submarine canyons. *Science Advances* **3** (10), e1700200.

Baker, M.L., Talling, P.J., Burnett, R., Pope, E.L., Ruffell, S., Urlaub, M., Clare, M.A., Jenkins, J., Dietze, M., Neasham, J., Silva Jacinto, R., Hage, S., Hasenhündl, M., Simmons, S.M., Heerema, C.J., Heijnen, M.S., Kunath, P., Cartigny, M.J.B., McGhee, C., Parsons, D.R. & Peirce, C. in review Seabed seismographs reveal nature of longest runout sediment flows on Earth. *Geophysical Research Letters* .

Balachandar, S., Salinas, Zuniga, Zuniga, S. & Cantero, M. 2024 A comprehensive understanding of the structure and dynamics of channelized turbidity currents. In *Particulate Gravity Currents in the Environment* (ed. Benjamin Kneller et al.), chap. 29. American Geophysical Union Monograph.

Biegert, Edward, Vowinckel, Bernhard, Ouillon, Raphael & Meiburg, Eckart 2017 High-resolution simulations of turbidity currents. *Progress in Earth and Planetary Science* **4** (1), 33.

Bolla Pittaluga, M., Frascati, A. & Falivene, O. 2018 A Gradually Varied Approach to Model Turbidity Currents in Submarine Channels. *Journal of Geophysical Research: Earth Surface* **123** (1), 80–96.

Bonnecaze, Roger T, Huppert, Herbert E & Lister, John R 1993 Particle-driven gravity currents. *Journal of Fluid Mechanics* **250**, 339–369.

Böttner, Christoph, Stevenson, Christopher J, Englert, Rebecca, Schönke, Mischa, Pandolpho, Bruna T, Geersen, Jacob, Feldens, Peter & Krastel, Sebastian 2024 Extreme erosion and bulking in a giant submarine gravity flow. *Science Advances* **10** (34), eadp2584.

Cantero, Mariano I., Balachandar, S., Cantelli, Alessandro, Pirmez, Carlos & Parker, Gary 2009*a* Turbidity current with a roof: Direct numerical simulation of self-stratified turbulent channel flow driven by suspended sediment. *Journal of Geophysical Research: Oceans* **114** (C3).

Cantero, Mariano I., Balachandar, S. & Parker, Gary 2009*b* Direct numerical simulation of stratification effects in a sediment-laden turbulent channel flow. *Journal of Turbulence* **10** (10), N27.

Cao, Z. X., Li, J., Pender, G. & Liu, Q. Q. 2015 Whole-Process Modeling of Reservoir Turbidity Currents by a Double Layer-Averaged Model. *Journal of Hydraulic Engineering* **141** (2), 04014069.

Covault, Jacob A., Fildani, Andrea, Romans, Brian W. & McHargue, Tim 2011 The natural range of submarine canyon-and-channel longitudinal profiles. *Geosphere* **7** (2), 313–332.

Curray, Joseph R, Emmel, Frans J & Moore, David G 2002 The Bengal Fan: morphology, geometry, stratigraphy, history and processes. *Marine and Petroleum Geology* **19** (10), 1191–1223.

Daly, R A 1936 Origin of submarine canyons. *American Journal of Science* **s5-31** (186), 401–420.

Deptuck, Mark E & Sylvester, Zoltán 2017 Submarine fans and their channels, levees, and lobes. In *Submarine Geomorphology*, *Springer Geology* 10, pp. 273–299. Cham: Springer.

Dorrell, R. M., Darby, S. E., Peakall, J., Sumner, E. J., Parsons, D. R. & Wynn, R. B. 2014 The critical role of stratification in submarine channels: Implications for channelization and long runout of flows. *Journal of Geophysical Research: Oceans* **119** (4), 2620–2641.

Eidsvik, Karl J. & Brørs, Bård 1989 Self-accelerated turbidity current prediction based upon $(k-\epsilon)$ turbulence. *Continental Shelf Research* **9** (7), 617–627.

Ellison, T. H. & Turner, J. S. 1959 Turbulent entrainment in stratified flows. *Journal of Fluid Mechanics* **6** (3), 423–448.

Fay, Gemma Louise 2012 Mathematical modelling of turbidity currents. PhD thesis, University of Oxford.

Fildani, A., Normark, W. R., Kostic, S. & Parker, G. 2006 Channel formation by flow stripping: large-scale scour features along the Monterey East Channel and their relation to sediment waves. *Sedimentology* **53** (6), 1265–1287.

Fukushima, Y., Parker, G. & Pantin, H. M. 1985 Prediction of Ignitive Turbidity Currents in Scripps Submarine-Canyon. *Marine Geology* **67** (1-2), 55–81.

Garcia, M. & Parker, G. 1989 Experiments on Hydraulic Jumps in Turbidity Currents near a Canyon-Fan Transition. *Science* **245** (4916), 393–396.

Garcia, M. & Parker, G. 1991 Entrainment of Bed Sediment into Suspension. *Journal of Hydraulic Engineering* **117** (4), 414–435.

Garcia, Marcelo H. 1994 Depositional Turbidity Currents Laden with Poorly Sorted Sediment. *Journal of Hydraulic Engineering* **120** (11), 1240–1263.

Halsey, Thomas C. & Kumar, Amit 2019 Levees Formed by Turbidity Currents: A Depth-Averaged Modeling Treatment. *Journal of Geophysical Research: Oceans* **124** (7), 4389–4415.

Hasenhündl, Martin, Talling, Peter J., Pope, Ed L., Baker, Megan L., Heijnen, Maarten S., Ruffell, Sean C., Jacinto, Ricardo da Silva, Gaillot, Arnaud, Hage, Sophie, Simmons, Stephen M., Heerema, Catharina J., McGhee, Claire, Clare, Michael A. & Cartigny, Matthieu J. B. 2024 Morphometric fingerprints and downslope evolution in bathymetric surveys: insights into morphodynamics of the Congo canyon-channel. *Frontiers in Earth Science* **12**, 1381019.

Heezen, B C & Ewing, W M 1952 Turbidity currents and submarine slumps, and the 1929 Grand Banks earthquake. *American Journal of Science* **250** (12), 849–873.

Heijnen, Maarten S., Clare, Michael A., Cartigny, Matthieu J. B., Talling, Peter J., Hage, Sophie, Lintern, D. Gwyn, Stacey, Cooper, Parsons, Daniel R., Simmons, Stephen M., Chen, Ye, Sumner, Esther J., Dix, Justin K. & Clarke, John E. Hughes 2020 Rapidly-migrating and internally-generated knickpoints can control submarine channel evolution. *Nature Communications* **11** (1), 3129.

Hsu, Shu-Kun, Kuo, Jackie, Lo, Chung-Liang, Tsai, Ching-Hui, Doo, Wen-Bin, Ku, Chia-Yen & Sibuet, Jean-Claude 2008 Turbidity Currents, Submarine Landslides and the 2006 Pingtung Earthquake off SW Taiwan. *Terrestrial, Atmospheric and Oceanic Sciences* **19** (6), 767.

Hu, P., Cao, Z. X., Pender, G. & Tan, G. M. 2012 Numerical modelling of turbidity currents in the Xiaolangdi reservoir, Yellow River, China. *Journal of Hydrology* **464**, 41–53.

Hu, Peng, Pähtz, Thomas & He, Zhiguo 2015 Is it appropriate to model turbidity currents with the three-equation model? *Journal of Geophysical Research: Earth Surface* **120** (7), 1153–1170, arXiv: 1505.07066.

Hughes Clarke, John E. 2016 First wide-angle view of channelized turbidity currents links migrating cyclic steps to flow characteristics. *Nature Communications* **7** (1), 11896.

Imran, J., Parker, G. & Katopodes, N. 1998 A numerical model of channel inception on submarine fans. *Journal of Geophysical Research-Oceans* **103** (C1), 1219–1238.

Imran, J., Parker, G. & Pirmez, C. 1999 A nonlinear model of flow in meandering submarine and subaerial channels. *Journal of Fluid Mechanics* **400**, 295–331.

Iwasaki, Toshiki & Parker, Gary 2020 The role of saltwater and waves in continental shelf formation with seaward migrating clinoform. *Proceedings of the National Academy of Sciences* **117** (3), 1266–1273.

Izumi, N. 2004 The formation of submarine gullies by turbidity currents. *Journal of Geophysical Research: Oceans* **109** (C3).

Jobe, Zane R., Howes, Nick C., Straub, Kyle M., Cai, Dingxin, Deng, Hang, Laugier, Fabien J., Pettinga, Luke A. & Shumaker, Lauren E. 2020 Comparing Aggradation, Superelevation, and Avulsion Frequency of Submarine and Fluvial Channels. *Frontiers in Earth Science* **8**, 53.

Johnson, Christopher G. & Hogg, Andrew J. 2013 Entraining gravity currents. *Journal of Fluid Mechanics* **731**, 477–508.

Konsoer, K., Zinger, J. & Parker, G. 2013 Bankfull hydraulic geometry of submarine channels created by turbidity currents: Relations between bankfull channel characteristics and formative flow discharge. *Journal of Geophysical Research-Earth Surface* **118** (1), 216–228.

Kostic, Svetlana & Parker, Gary 2006 The response of turbidity currents to a canyon–fan transition: internal hydraulic jumps and depositional signatures. *Journal of Hydraulic Research* **44** (5), 631–653.

Kuenen, Ph. H. 1938 Density Currents in connection with the problem of Submarine Canyons. *Geological Magazine* **75** (6), 241–249.

Lamb, Michael P, Dietrich, William E & Sklar, Leonard S 2008 A model for fluvial bedrock incision by impacting suspended and bed load sediment. *Journal of Geophysical Research: Earth Surface (2003–2012)* **113** (F3).

Lamb, M. P., Hickson, T., Marr, J. G., Sheets, B., Paola, C. & Parker, G. 2004 Surging versus continuous turbidity currents: Flow dynamics and deposits in an experimental intraslope minibasin. *Journal of Sedimentary Research* **74** (1), 148–155.

Lamb, M. P., Toniolo, H. & Parker, G. 2006 Trapping of sustained turbidity currents by intraslope minibasins. *Sedimentology* **53** (1), 147–160.

Luchi, R., Balachandar, S., Seminara, G. & Parker, G. 2018 Turbidity currents with equilibrium basal driving layers: a mechanism for long runout. *Geophysical Research Letters* **45** (3), 1518–1526.

Ma, Hongbo, Nittrouer, Jeffrey A., Wu, Baosheng, Lamb, Michael P., Zhang, Yuanfeng, Mohrig, David, Fu, Xudong, Naito, Kensuke, Wang, Yuanjian, Moodie, Andrew J., Wang, Guangqian, Hu, Chunhong & Parker, Gary 2020 Universal relation with regime transition for sediment transport in fine-grained rivers. *Proceedings of the National Academy of Sciences* **117** (1), 171–176.

Ma, H. B., Nittrouer, J. A., Naito, K., Fu, X. D., Zhang, Y. F., Moodie, A. J., Wang, Y. J., Wu, B. S. & Parker, G. 2017 The exceptional sediment load of fine-grained dispersal systems: Example of the Yellow River, China. *Science Advances* **3** (5), e1603114.

Meiburg, Eckart & Kneller, Ben 2010 Turbidity Currents and Their Deposits. *Annual Review of Fluid Mechanics* **42** (1), 135–156.

Mikkelsen, N, Maslin, M, Giraudeau, J & Showers, W 1997 Biostratigraphy and sedimentation rates of the Amazon Fan. In *Proc. of the Ocean Drilling Program*, *Proceedings of the Ocean Drilling Program* Chapter 38. Ocean Drilling Program.

Pantin, H. M. 1979 Interaction between velocity and effective density in turbidity flow: Phase-plane analysis, with criteria for autosuspension. *Marine Geology* **31** (1-2), 59–99.

Parker, G. 1982 Conditions for the Ignition of Catastrophically Erosive Turbidity Currents. *Marine Geology* **46** (3-4), 307–327.

Parker, G., Fukushima, Y. & Pantin, H. M. 1986 Self-Accelerating Turbidity Currents. *Journal of Fluid Mechanics* **171** (-1), 145–181.

Parker, G., Garcia, M., Fukushima, Y. & Yu, W. 1987 Experiments on turbidity currents over an erodible bed. *Journal of Hydraulic Research* **25** (1), 123–147.

Paull, Charles K., Talling, Peter J., Maier, Katherine L., Parsons, Daniel, Xu, Jingping, Caress, David W., Gwiazda, Roberto, Lundsten, Eve M., Anderson, Krystle, Barry, James P., Chaffey, Mark, O'Reilly, Tom, Rosenberger, Kurt J., Gales, Jenny A., Kieft, Brian, McGann, Mary, Simmons, Steve M., McCann, Mike, Sumner, Esther J., Clare, Michael A. & Cartigny, Matthieu J. 2018 Powerful turbidity currents driven by dense basal layers. *Nature Communications* **9** (1), 4114.

Picot, M., Droz, L., Marsset, T., Dennielou, B. & Bez, M. 2016 Controls on turbidite sedimentation: Insights from a quantitative approach of submarine channel and lobe architecture (Late Quaternary Congo Fan). *Marine and Petroleum Geology* **72**, 423–446.

Pirmez, Carlos & Imran, Jasim 2003 Reconstruction of turbidity currents in Amazon Channel. *Marine and Petroleum Geology* **20** (6-8), 823–849.

Pope, Ed L., Cartigny, Matthieu J. B., Clare, Michael A., Talling, Peter J., Lintern, D. Gwyn, Vellinga, Age, Hage, Sophie, Açikalin, Sanem, Bailey, Lewis, Chapplow, Natasha, Chen, Ye, Eggenhuisen, Joris T., Hendry, Alison, Heerema, Catharina J., Heijnen, Maarten S., Hubbard, Stephen M., Hunt, James E., McGhee, Claire, Parsons, Daniel R., Simmons, Stephen M., Stacey, Cooper D. & Vendettuoli, Daniela 2022 First source-to-sink monitoring shows dense head controls sediment flux and runout in turbidity currents. *Science Advances* **8** (20), eabj3220.

Rajaratnam, N 1976 Turbulent Jets. *Developments in Water Science* 5, pp. v–vi. Elsevier Science.

Reece, J. Kevin, Dorrell, Robert M. & Straub, Kyle M. 2024 Circulation of hydraulically ponded turbidity currents and the filling of continental slope minibasins. *Nature Communications* **15** (1), 2075.

Ribberink, Jan S. 1998 Bed-load transport for steady flows and unsteady oscillatory flows. *Coastal Engineering* **34** (1-2), 59–82.

Salaheldin, T.M., Imran, J., Chaudhry, M.H. & Reed, C. 2000 Role of fine-grained sediment in turbidity current flow dynamics and resulting deposits. *Marine Geology* **171** (1-4), 21–38.

Salinas, Jorge, Balachandar, S., Shringarpure, Mrugesh, Fedele, Juan, Hoyal, David & Cantero, Mariano 2020 Soft transition between subcritical and supercritical currents through intermittent cascading interfacial instabilities. *Proceedings of the National Academy of Sciences* **117** (31), 18278–18284.

Salinas, Jorge S., Balachandar, S. & Cantero, M. I. 2021*a* Control of turbulent transport in supercritical currents by three families of hairpin vortices. *Physical Review Fluids* **6** (6), 063801.

Salinas, Jorge S., Balachandar, S., Shringarpure, M., Fedele, J., Hoyal, D., Zuñiga, S. & Cantero, M. I. 2021*b* Anatomy of subcritical submarine flows with a lutocline and an intermediate destruction layer. *Nature Communications* **12** (1), 1649.

Salinas, Jorge S., Cantero, M. I., Shringarpure, M. & Balachandar, S. 2019*a* Properties of the Body of a Turbidity Current at Near-Normal Conditions: 1. Effect of Bed Slope. *Journal of Geophysical Research: Oceans* **124** (11), 7989–8016.

Salinas, Jorge S., Cantero, M. I., Shringarpure, M. & Balachandar, S. 2019*b* Properties of the Body of a Turbidity Current at Near-Normal Conditions: 2. Effect of Settling. *Journal of Geophysical Research: Oceans* **124** (11), 8017–8035.

Salinas, Jorge S., Zúñiga, Santiago, Cantero, M.I., Shringarpure, M., Fedele, J., Hoyal, D. & Balachandar, S. 2022 Slope dependence of self-similar structure and entrainment in gravity currents. *Journal of Fluid Mechanics* **934**, R4.

Schwenk, Tilmann, Spieß, Volkhard, Hübscher, Christian & Breitzke, Monika 2003 Frequent channel avulsions within the active channel–levee system of the middle Bengal Fan—an exceptional channel–levee development derived from Parasound and Hydrosweep data. *Deep Sea Research Part II: Topical Studies in Oceanography* **50** (5), 1023–1045.

Sequeiros, O. E., Cantelli, A., Viparelli, E., White, J. D. L., Garcia, M. H. & Parker, G. 2009 Modeling turbidity currents with nonuniform sediment and reverse buoyancy. *Water Resources Research* **45** (6).

Simmons, S. M., Azpiroz-Zabala, M., Cartigny, M. J .B., Clare, M. A., Cooper, C., Parsons, D. R., Pope, E. L., Sumner, E. J. & Talling, P. J. 2020 Novel Acoustic Method Provides First Detailed Measurements of Sediment Concentration Structure Within Submarine Turbidity Currents. *Journal of Geophysical Research: Oceans* **125** (5), e2019JC015904.

Skevington, Edward W G & Dorrell, Robert M 2024 Self-stratifying turbidity currents. *arXiv* , arXiv: 2207.13826.

Spinewine, Benoit & Capart, Hervé 2013 Intense bed-load due to a sudden dam-break. *Journal of Fluid Mechanics* **731**, 579–614.

Spinewine, Benoit, Sun, Tao, Babonneau, Nathalie & Parker, Gary 2011 Self-similar long profiles of aggrading submarine leveed channels: Analytical solution and its application to the Amazon channel. *Journal of Geophysical Research: Earth Surface* **116** (F3).

Sumner, E. J., Peakall, J., Parsons, D. R., Wynn, R. B., Darby, S. E., Dorrell, R. M., McPhail, S. D., Perrett, J., Webb, A. & White, D. 2013 First direct measurements of hydraulic jumps in an active submarine density current. *Geophysical Research Letters* **40** (22), 5904–5908.

Symons, William O., Sumner, Esther J., Paull, Charles K., Cartigny, Matthieu J.B., Xu, J.P., Maier, Katherine L., Lorenson, Thomas D. & Talling, Peter J. 2017 A new model for turbidity current behavior based on integration of flow monitoring and precision coring in a submarine canyon. *Geology* **45** (4), 367–370.

Talling, Peter J., Baker, Megan L., Pope, Ed L., Ruffell, Sean C., Jacinto, Ricardo Silva, Heijnen, Maarten S., Hage, Sophie, Simmons, Stephen M., Hasenhündl, Martin, Heerema, Catharina J., McGhee, Claire, Apprioual, Ronan, Ferrant, Anthony, Cartigny, Matthieu J. B., Parsons, Daniel R., Clare, Michael A., Tshimanga, Raphael M., Trigg, Mark A., Cula, Costa A., Faria, Rui, Gaillot, Arnaud, Bola, Gode, Wallance, Dec, Griffiths, Allan, Nunny, Robert, Urlaub, Morelia, Peirce, Christine, Burnett, Richard, Neasham, Jeffrey & Hilton, Robert J. 2022 Longest sediment flows yet measured show how major rivers connect efficiently to deep sea. *Nature Communications* **13** (1), 4193.

Toniolo, H., Lamb, M. & Parker, G. 2006*a* Depositional turbidity currents in diapiric minibasins on the continental slope: Formulation and theory. *Journal of Sedimentary Research* **76** (5), 783–797.

Toniolo, H., Parker, G., Voller, V. & Beaubouef, R. T. 2006*b* Depositional turbidity currents in diapiric minibasins on the continental slope: Experiments - Numerical simulation and upscaling. *Journal of Sedimentary Research* **76** (5), 798–818.

Traer, M. M., Fildani, A., Fringer, O., McHargue, T. & Hilley, G. E. 2018*a* Turbidity Current Dynamics: 1. Model Formulation and Identification of Flow Equilibrium Conditions Resulting From Flow Stripping and Overspill. *Journal of Geophysical Research: Earth Surface* **123** (3), 501–519.

Traer, M. M., Fildani, A., Fringer, O., McHargue, T. & Hilley, G. E. 2018*b* Turbidity Current Dynamics: 2. Simulating Flow Evolution Toward Equilibrium in Idealized Channels. *Journal of Geophysical Research: Earth Surface* **123** (3), 520–534.

Wahab, Abdul, Hoyal, David C., Shringarpure, Mrugesh & Straub, Kyle M. 2022 A dimensionless framework for predicting submarine fan morphology. *Nature Communications* **13** (1), 7563.

Wang, Zhiwen, Xu, Jingping, Talling, Peter J., Cartigny, Matthieu J. B., Simmons, Stephen M., Gwiazda, Roberto, Paull, Charles K., Maier, Katherine L. & Parsons, Daniel R. 2020 Direct evidence of a high-concentration basal layer in a submarine turbidity current. *Deep Sea Research Part I: Oceanographic Research Papers* **161**, 103300.

Wetzel, Andreas 1993 The Transfer of River Load to Deep-Sea Fans: A Quantitative Approach. *AAPG Bulletin* **77**.

Wu, Zhuyuan & Izumi, Norihiro 2022 Transportational Cyclic Steps Created by Submarine Long-Runout Turbidity Currents. *Geosciences* **12** (7), 263.

Xie, Jiafeng, Hu, Peng, Zhu, Chenlin, Yu, Zhaosheng & Pähtz, Thomas 2023*a* Turbidity currents propagating down an inclined slope: particle auto-suspension. *arXiv* , arXiv: 2302.01755.

Xie, Jiafeng, Zhu, Chenlin, Hu, Peng, Yu, Zhaosheng & Pan, Dingyi 2023*b* Particle segregation within bidisperse turbidity current evolution. *Journal of Fluid Mechanics* **971**, A16.

Xu, J. P., Noble, M. A. & Rosenfeld, L. K. 2004 In-situ measurements of velocity structure within turbidity currents. *Geophysical Research Letters* **31** (9).

Yeh, Tzu-hao, Cantero, Mariano, Cantelli, Alessandro, Pirmez, Carlos & Parker, Gary 2013 Turbidity current with a roof: Success and failure of RANS modeling for turbidity currents under strongly stratified conditions. *Journal of Geophysical Research: Earth Surface* **118** (3), 1975–1998.

Zhang, Li, Parker, Gary, Izumi, Norihiro, Cartigny, Matthieu, Li, Tiejian & Wang, Guangqian 2017 Morphodynamic Model of Submarine Canyon Incision by Sandblasting. In *AGU Fall Meeting*, , vol. 2017, pp. EP13C–1645.